Dendrogeomorphic reconstruction of floods in a dynamic tropical river

Article *in* Geomorphology · March 2020

DOI: 10.1016/j.geomorph.2020.107133

5 authors, including:

Adolfo Quesada-Román
University of Geneva
82 PUBLICATIONS **330** CITATIONS
SEE PROFILE

Juan Antonio Ballesteros-Canovas
University of Geneva
165 PUBLICATIONS **2,117** CITATIONS
SEE PROFILE

Sebastián Granados
University of Costa Rica
7 PUBLICATIONS **12** CITATIONS
SEE PROFILE

Christian Birkel
University of Costa Rica
157 PUBLICATIONS **2,070** CITATIONS
SEE PROFILE

Geomorphology 359 (2020) 107133

Contents lists available at ScienceDirect

Geomorphology

journal homepage: www.elsevier.com/locate/geomorph

Dendrogeomorphic reconstruction of floods in a dynamic tropical river

Adolfo Quesada-Román [a,b,c,*], Juan Antonio Ballesteros-Cánovas [a,c], Sebastián Granados-Bolaños [b], Christian Birkel [b], Markus Stoffel [a,c,d]

[a] Climatic Change Impacts and Risks in the Anthropocene (C-CIA), Institute for Environmental Sciences, University of Geneva, Boulevard Carl-Vogt 66, CH-1205 Geneva, Switzerland
[b] Department of Geography and Water and Global Change Observatory, University of Costa Rica, 2060 San José, Costa Rica
[c] Dendrolab.ch, Department of Earth Sciences, University of Geneva, 13 rue des Maraîchers, CH-1205 Geneva, Switzerland
[d] Department F.-A. Forel for Environmental and Aquatic Sciences, University of Geneva, Geneva, Switzerland

ARTICLE INFO

Article history:
Received 4 October 2019
Received in revised form 26 February 2020
Accepted 27 February 2020
Available online 05 March 2020

Keywords:
Dendrogeomorphology
Fluvial geomorphology
Hydraulic modelling
Tropics

ABSTRACT

Tropical regions are frequently affected by intense floods causing substantial human and economic losses. A proper management of floods and the prevention of disasters is, however, often hampered by a generalized paucity of systematic discharge measurements, which in turn renders any assessment of the frequency and magnitude of extreme floods challenging or impossible. Here, we analyze the suitability of trees impacted by floods and their growth-ring records to provide insights into past flood activity and to allow estimation of their magnitude. We base this exploratory study on the extreme floods triggered by the passage of tropical storm Nate on October 5, 2017 and investigate whether dendrogeomorphic approaches can be employed to date and quantify floods in the catchment of tropical Río General (Costa Rica). To this end, we sampled 91 trees showing scars in three river reaches and tested their potential to serve as paleostage indicators (PSI). High-resolution (0.5 m) digital surface and elevation models were then obtained with an Unmanned Aerial Vehicle to run a step-backwater hydraulic simulation aimed at defining flood peak discharge for which the mean squared errors between PSI heights and simulated water tables could be minimized. In a last analytical step, we investigated which hydraulic (i.e., Froude number, flow velocity) and fluvial landform characteristics explained deviations between scar heights and modeled water tables best by using a generalized linear model. Our analysis confirms that scarred trees can indeed be used for the reconstruction of past floods in tropical river systems and that the geomorphic position of trees will exert control on deviations between modeled water tables and scar height, with cut banks being most suited for scar-based flood reconstruction.

1. Introduction

Tropical mountain zones are densely populated, and land-use changes led to increased vulnerability to extreme weather-related hazards (Lawrence and Vandecar, 2015; Slaymaker and Embleton-Hamann, 2018). Land-use changes enhance stream water and sediment yields, changing sediment dynamics, bed and bank stability, and channel geometry (Wohl, 2006). The seasonally or perennially barotropic conditions that dominate tropical climates are the Intertropical Convergence Zone where the trade winds, cold fronts, cyclonic systems, and orographic uplift converge (Wohl, 2008). In addition, floods in the tropics behave as the combined interaction of land-use change and climatological dynamics associated with intense seasonal and extraordinary rainfall events (Syvitski et al., 2014). As a result of greater inputs and faster rates of change in the tropics compared to e.g., temperate regions, the hydrological processes that cause extreme streamflow events and flash floods are also accelerated (Wohl et al., 2012).

Flood assessments require accurate information on the spatial and temporal distribution of rainfall and on the resulting discharge (Baker, 2008). Such information is often scarce and of poor quality, even more so in tropical countries for which information on hydrological monitoring and measurements are often lacking completely (Wohl et al., 2012). The generalized lack of data availability calls for alternative approaches that allow adequate estimation of peak discharges of past flood events.

In the days and weeks after a flood, flood marks left in the field can be used to estimate the extent and magnitude of a flood. Flood marks are, however, highly perishable and often disappear within a few months (Borga et al., 2008, 2014). Botanical indicators typically cover much longer time windows and can therefore serve as a relevant source of evidence to date floods and to quantify their magnitude in rivers with insufficient or nonexistent gauge records (Sigafoos, 1964; Ballesteros-Cánovas et al., 2015b). Thereby, woody plants are used as palaeoflood indicators on the basis of the "process–event–response" concept, in which a specific flood represents the "process" and the resulting tree

* Corresponding author at: Department of Geography and Water and Global Change Observatory, University of Costa Rica, 2060 San José, Costa Rica.
E-mail address: adolfo.quesada@unige.ch (A. Quesada-Román).

https://doi.org/10.1016/j.geomorph.2020.107133
0169-555X/

disturbance is considered an "event" in the tree-ring series (Shroder, 1978; Wilhelm et al., 2019). Botanical evidence of past floods includes exposed roots, tilted trunks and mutilated branches of trees growing along river corridors (Gottesfeld and Gottesfeld, 1990; Stoffel and Wilford, 2012; Díez-Herrero et al., 2013). Scars in trees constitute the most reliable indicator of past floods as they allow precise dating of the event as well as a determination of water stages during floods (Gottesfeld, 1996; Ballesteros-Cánovas et al., 2011a, 2011b). The use of tree-ring records in river corridors has allowed the extension of flood records back in time in various rivers, but past research has focused mostly on temperate mountain environments (Sigafoos, 1964; McCord, 1990; Ballesteros-Cánovas et al., 2015b; Wilhelm et al., 2019). In addition to "conventional" floods, tree-ring records have also been used to date ice jam (Smith and Reynolds, 1983; Lagadec et al., 2015) or lahar events (Franco-Ramos et al., 2020). After its initial application in North America, the approach has since been employed in various catchments of the Iberian Peninsula (Ruiz-Villanueva et al., 2013; Rodriguez-Morata et al., 2016), Central Europe (Zielonka et al., 2008; Ballesteros-Cánovas et al., 2015a, 2016), and the Himalayas (Ballesteros-Cánovas et al., 2017; Speer et al., 2019).

Some uncertainties, however, remain in the dendrogeomorphic assessment and interpretation of past floods. For instance, uncertainties still persist regarding the most suitable locations for the sampling of scars that would allow the minimization of deviations between real and reconstructed flood heights (Ballesteros-Cánovas et al., 2015a; Victoriano et al., 2018). In addition, despite substantial advances realized in the field of palaeoflood reconstructions, to our best knowledge, scars in trees have not been used so far to reconstruct floods in the tropics, probably because of inherent difficulties in correctly analyzing growth ring records from tropical trees (Silva et al., 2019).

In this paper, we therefore aim to test the suitability of tropical trees for the reconstruction of the magnitude of a recent extreme flood in Costa Rica that was caused by the passage of tropical storm Nate. The focus of this study is on channel segments of Río General, Costa Rica. We apply dendrogeomorphic approaches to study (i) the potential for tropical trees to record evidence of past floods, (ii) the effects of tree position on peak discharge reconstructions, so as to (iii) identify relations among as well as dependencies between hydrological and dendrogeomorphic variables in reconstructions, with the aim to inform future studies on how to improve sampling of trees for flood peak discharge reconstructions.

2. Study area

2.1. Geographic setting

Río General (or General River) has a length of 23 km for a catchment size of 316 km^2, with a channel slope of 8.22°, and a mean annual bankfull discharge (1970–2019) of 222 m^3/s. Río General is one of the main tributaries of the Térraba River, the largest catchment of Costa Rica (Quesada-Román and Zamorano-Orozco, 2019a; Camacho et al., 2020). The river drains the Pacific slopes of the Cordillera de Talamanca and has its source at the highest peak of the country (Quesada-Román et al., 2019b), Cerro Chirripó (3810 m asl), and flows into the Térraba River at 800 m asl, thus covering an altitudinal range of >3 km.

The three reaches of the Río General investigated in this study have mainly braided channel morphologies that consist primarily of cobbles and boulders and are located around the central coordinates 9.432°N and −83.638°W (Fig. 1). The tree sites are representative of the larger study region and show a high density of scarred trees suitable for dendrogeomorphic analyses: whereas site A is located in the Buenavista tributary of Río General, sites B and C are found in the Chirripó Pacífico tributary.

Vegetation is composed mostly of tropical premontane rainforests with evidence of deforestation (slash-burning) and landscape fragmentation dating back to the 1950s. Even if anthropogenic changes continued into mid-1980s, deforestation locally reached its peak during the 1960s and 1970s. In 1996, a deforestation ban was put into force. Together with the rise of ecotourism and the development of more sustainable production alternatives, this ban has contributed to the recovery of the ecosystem (Kappelle, 2016; Krishnaswamy et al., 2018).

According to the National Forestry Inventory, the average square hectare in this region contains 16 species with a mean diameter at breast height (DBH) of 20.8 cm, as well as at least 40 individuals with a DBH > 10 cm. According to the same data, mean Stand Basal Area (SBA) corresponds to 1.64 m^2 (REDD/CCAD-GIZ - SINAC, 2015).

2.2. Climate characteristics and tropical cyclone activity

The latitudinal migration of the Intertropical Convergence Zone (ITCZ), the El Niño Southern Oscillation (ENSO), northeast trade winds, cold fronts, and tropical cyclones influence the local climate and precipitation patterns (Alfaro et al., 2010; Campos-Durán and Quesada-Román, 2017). Annual rainfall totals typically reach 3000–5000 mm in the region with two distinct rainfall maxima, one in May and a second, more distinct rainfall peak in October. In July and August, rainfall decreases during two to four weeks, known as the Mid-Summer Drought (Maldonado et al., 2016; Quesada-Román, 2017). About 85% of the annual rainfall occurs between May and November (rainy season) with a distinct dry season from December to April. Annual average temperatures range between 18 and 22 °C at the study site (Quesada-Román and Zamorano-Orozco, 2018, 2019b).

Floods can be favored by intense local convection, but historically the most severe floods were triggered by tropical cyclones. The 2017 North Atlantic hurricane season was very active, with anomalously warm sea surface temperatures in the tropical Atlantic and neutral-to-colder La Niña conditions in the tropical Pacific (NOAA, 2019). Normally, these conditions are favorable to the formation of hurricanes in the Atlantic basin (Goldenberg et al., 2001).

The focus of this study is on tropical storm "Nate" because it caused an extreme discharge event in the General River catchment. Nate originated from a large area of low pressure in the eastern Pacific ITCZ and over Central America that gradually developed in early October (Papin et al., 2017; Beven and Berg, 2018).

Tropical cyclones are one of the main triggers of floods in General River and produce events every nine years on average. Historical discharges have increased gradually between Hurricane Joan in 1988 (597 m^3/s), Hurricane Cesar in 1996 (~650–700 m^3/s), and Tropical Storm Alma in 2008 (756 m^3/s; Cervantes-Cordero, 1999; ICE, 2018). Prior to the passage of Nate, Costa Rica already experienced intense rainfall for over two weeks under the influence of the ITCZ. These conditions of antecedent soil wetness in combination with intense and prolonged rainfall during the passage of Nate (200–500 mm) triggered floods and landslides across the country (CNE, 2018). At the study site, between 300 and 400 mm of rainfall had been recorded between October 4–8, 2017 (Beven and Berg, 2018), resulting in an observed discharge peak of 947 m^3/s. The 2017 Río General flood lasted from October 4–10 and had a total flow volume of 124 Hm^3 (ICE, 2018). Nate impacted 85% of the Costa Rican territory with widespread landsliding and flooding, causing 11 fatalities and economic losses of US$ 578 million (CNE, 2018), or 1.3% of the Gross Domestic Product (Brenes and Girot, 2018).

3. Material and methods

3.1. Experimental work and dendrogeomorphic techniques

We surveyed a total of 91 scarred trees at three different study reaches of the Río General in January 2018, i.e., only two months after the passage of Nate and the flood event (Fig. 1). In the field, we only sampled scars that could be attributed clearly to past flooding to avoid any biases for the subsequent peak discharge reconstruction

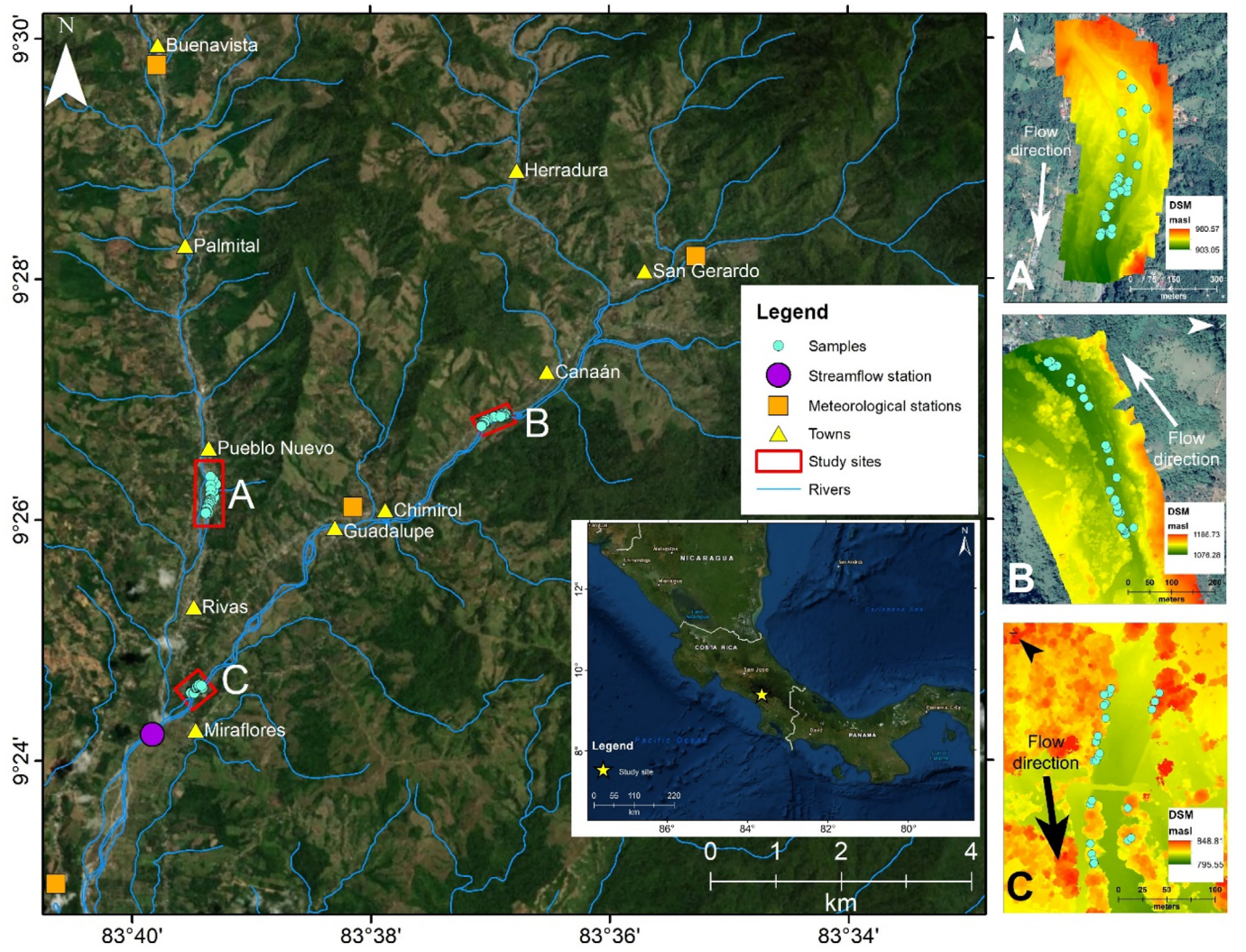

Fig. 1. Location of the three study reaches (A, B, and C) within the Río General catchment, streamflow station, meteorological stations, towns and drainage network. The right panels present the Digital Surface Models derived from Unmanned Aerial Vehicle photogrammetry as well as the location of trees sampled.

(Ballesteros-Cánovas et al., 2015a). Criteria used for the selection of scars were defined as follows: scars (i) were inflicted by the flood triggered by Nate, (ii) had to face the direction of flow, and (iii) had to exhibit a shape typical of flood impacts (Sigafoos, 1964; Hupp, 1988; Ballesteros-Cánovas et al., 2011a).

All scars fulfilling these criteria were considered as paleostage indicators (PSI), their position recorded with a Global Positioning System (GPS; precision of <1 m) and scar height with respect to the channel measured as the central height of the injury from tree base (Ballesteros-Cánovas et al., 2011b). In addition, a preliminary geomorphic map was derived from images obtained with Unmanned Aerial Vehicle (UAV) High Resolution Photogrammetry, with the aim to identify different fluvial landforms at the study sites (Smith et al., 2011).

In a further step, we classified trees according to their geomorphic position (Leopold et al., 1995; Wheaton et al., 2015) within the floodplain. To this end, we classified tree positions according to their location on cut bank (CB), point bar (PB), and straight channel (SC) segments within the study reaches (Fig. 2).

3.2. Hydraulic modelling, peak discharge estimation and regression analysis

The two-dimensional (2D) hydrodynamic model IBER (www.iberaula.es) was used to model water depth, Froude number, and flow velocities of the flood event of 2017. IBER simulates turbulent-free, unsteady surface flows and environmental processes in rivers by solving depth-averaged 2D shallow water equations (2D Saint-Venant) using a finite volume method with a second-order roe scheme (Cea et al., 2019). This approach is particularly suitable for flows in mountain streams where shocks and discontinuities can occur, and where flow hydrographs tend to be flashy. The method is conservative, even in cases where wetting and drying processes occur. The model works in a non-structured mesh consisting of triangles or quadrilateral elements. In our study, we used high resolution UAV elevational data obtained from digital imagery. A Structure from Motion (SfM) approach was applied to obtain georectified orthomosaics and digital elevation models (Turner et al., 2012). Digital images were obtained with a DJI Phantom 4 Pro V2 drone. The photogrammetric reconstruction of the fluvial environments for hydraulic modelling and point cloud classification was realized using Agisoft Photoscan 1.4.0 so as to generate precise elevation models for environmental analysis (Langhammer and Vacková, 2018).

Bed friction was evaluated in the field with Manning's n roughness coefficient considering homogenous roughness units (Chow, 1959). We used a Manning's $n = 0.075$ for the main channel, 0.16 for the forest, and 0.08 for those sectors with sparse vegetation (Barnes, 1967; Arcement and Schneider, 1989). To compute the inlet water discharge (i.e., steady flow regime), velocity and Froude number (Fr) into each study reach, we thereafter modeled successive inlet discharges based on historical extremes (using steps of 100 m^3/s up to 1500 m^3/s).

Fig. 2. Representative scarred tree individuals affected by the flood triggered by Tropical Storm Nate on point bars of Site A (a) as well as on cut banks of Sites A and C, respectively (b, d). Example (c) characterizes scarred trees growing in a straight channel of Site B.

Peak discharge of the 2017 flood was simulated with an iterative step-backwater procedure and consisted of a (i) calculation of water stages from modeled peak discharges and (ii) a fitting of resulting modeled water surfaces with PSI heights identified in the field (Webb and Jarrett, 2002). For more robust flood discharge estimations, we then calculated the mean squared error (MSE) of each modeled discharge output against every scar height. The magnitude of the flood event in each river reach was then defined as the peak discharge for which the MSE between the model and scar heights was smallest (Fig. 3).

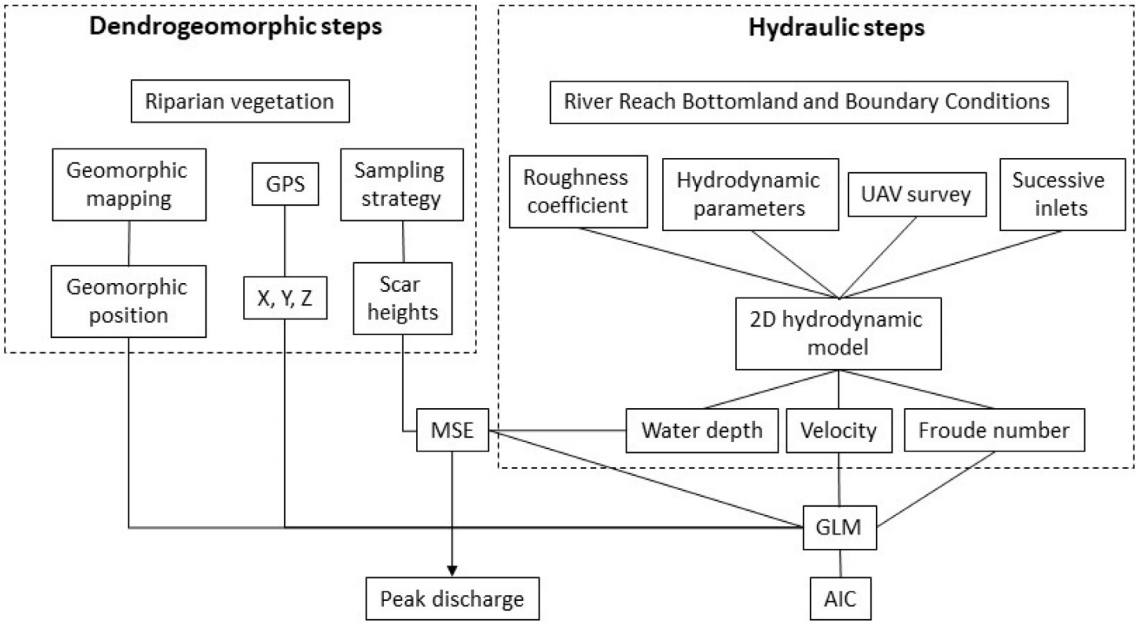

Fig. 3. Methodological diagram used for the assessment of locations that are best suited for palaeoflood discharge reconstruction.

Thereafter, we analyzed combinations of hydraulic and geomorphic characteristics for which the MSE between modeled flow heights and scar heights was smallest at the level of individual trees. We therefore applied a least squares regression analysis to calculate peak discharges at each of the three study reaches. With the help of a generalized linear models (GLM), we then described the MSE of each tree statistically by adding the Froude number (as an indicator of flow regime) and the geomorphic position (or landform) of trees at each site (A, B, and C). To this end, all variables were transformed into z-scores. The Akaike Information Criterion (AIC; Anderson and Burnham, 2004) was used in a backward selection to contrast the full hypothesis

MSE ~ Froude × (*Landform* + *Site*), for which an interaction between the hydraulic and landform variables is defined, against the alternative hypothesis, where only landform is considered: *MSE ~ Landform* + *Site*. Model parameters were then used to evaluate the weight of each co-variable to define the most suitable landform for tree sampling in (tropical) mountain rivers.

4. Results

4.1. Peak discharge reconstruction based on scars in tropical trees

A total of 91 trees showed visible scars that were inflicted by sediment and wood transported during the flood triggered by tropical storm Nate; 29 scars were identified in sector A, 31 in B, and 31 in C. Mean scar heights were similar for all trees that were considered for peak discharge reconstruction with 2.32 m ($\sigma = 0.76$, Table 1). On average, the highest scar heights were recorded in reach B (2.57 ± 0.731 m above the channel bed), whereas the lowest scar heights were found in reach C (2.15 ± 0.784 m). The positions of scarred trees with respect to cut banks (CB), point bars (PB) and straight channels (SC) are presented in Table 1.

The hydraulic model points to differing hydraulic conditions prevailing at the three sites during the 2017 flood induced by tropical storm Nate (Fig. 4). Site A presents a peak discharge of 636 m^3/s ($\sigma = 0.16$) with a mean water depth of 1.87 m, an average velocity of 2.37 m/s, a mean Froude number of 0.54, and absolute deviations between modeled flow heights and scar heights ranging from −2.27 to 2.79 m. Site B shows a peak discharge of 455 m^3/s ($\sigma = 0.24$) with a mean water depth of 2.33 m, an average flow velocity of 2.35 m/s, a mean Froude number of 0.70, and absolute deviations between modeled flow heights and scar heights of −3.01 to 3.30 m. Site C has a peak discharge of 1249 m^3/s ($\sigma = 0.43$) with a mean water depth of 3.18 m, an average flow velocity of 2.23 m/s, a mean Froude number of 0.43, and absolute deviations between modeled flow heights and scar heights between −2.86 and 2.57 m. The reconstructed high flows correspond with observations at the gauging station at which a discharge of 947 m^3/s was measured.

4.2. Fluvial and dendrogeomorphic factors controlling deviations between field and model data

Statistical analyses of the average mean squared error between the reconstructed and modeled flood peak discharge were analyzed with the AIC criterion. Our results support the alternative model with $AIC_{Ha} = 31.65$ against the null hypothesis (*MSE ~ Froude* × (*Landform* + *Froude*) × *Site*; $AIC_{Hf} = 32.16$) and suggest that the best generalized linear model supports an interaction between the geomorphic position of sampled trees and study reach (*MSE ~ Landform* + *Site*). Table 2 provides the model parameters, but also indicates that the most significant influence on flood peak discharge probability is given by the straight channel as well as Site B and C, as shown by the z-ratio tests of parameter estimates.

Results also show that trees scarred at cut banks have the smallest MSE (~1.52) and best fit with peak discharge reconstructions, whereas for scars in trees located at point bars (~1.78) generally exhibited larger MSE and can thus be considered less reliable for peak discharge reconstructions based on dendrogeomorphic evidence (Fig. 5).

In line with the GLM, the relation of the Froude number with the MSE varied with geomorphic position (Fig. 6). Point bars showed an increase of MSE as the Froude number increases, whereas in the case of straight channels, no such tendency could be found. At cut banks, MSE decreased with increasing Froude numbers. The geomorphic position also influences modeled flow velocity and shear stress. As such, point bars often show the smallest flow velocities and shear stress but are also more easily transformed or destroyed during the flood. In the case of straight channels, morphology constantly changes during floods as well. In addition, the highest velocity and shear stresses are found within the main channel where trees are not commonly present. Cut banks are characterized by strong flow velocities and shear stress as well, but the intermittent, progressive erosion still favors tree growth on river banks, rendering these ideal sites to sample flood scars in trees.

Table 1
Characteristics of the scars used as paleostage indicators (PSI) for each of the study reaches. Abbreviations: MSE — mean squared error; SC — straight channel; PB — point bar; CB — cut bank.

Study reach	Scars in trees	Scar heights (m)	MSE	Tree positions (%)
A	29	2.25 ± 0.70	1.46	SC = 41, PB = 21, CB = 38
B	31	2.57 ± 0.73	1.64	SC = 29, PB = 19, CB = 52
C	31	2.15 ± 0.78	2.10	SC = 38, PB = 21, CB = 41

5. Discussion

In this contribution, we provide a scar-based flow discharge reconstruction for three floodplain sections of the General River, southeastern Costa Rica. In particular, we analyzed 91 trees with clear flood-induced scars and used a 2D hydraulic model run on a highly-resolved topography to estimate peak discharge of the extraordinary 2017 flood triggered by the passage of Tropical Storm Nate in October 2017. Moreover, we investigated the role of relative tree positions on the quality of flow discharge reconstructions and searched for ways to reduce deviations between modeled and reconstructed peak discharges.

5.1. Methodological uncertainties

In regions where baseline data on floods are lacking, one must limit all other sources of possible uncertainties to obtain the best results. One such possible source of uncertainties is related to topography on which hydraulic models are run. In this study, good precision of hydraulic models could be achieved thanks to the use of high-resolution orthoimages obtained from UAV photogrammetry (Perks et al., 2016). Based on the highly resolved topography, the MSE between modeled water stages and the height of scars could be limited to 1.25 m on average between the three reaches analyzed. These results are comparable to those obtained at sites in Poland based on the same 2D-hydraulic model (~0.8 m; Ballesteros-Cánovas et al., 2016). Yanosky and Jarrett (2002) observed deviations ranging from −0.6 to 1.5 m in a high-gradient stream, whereas Gottesfeld (1996) obtained 0.196 ± 0.03 m error variations in low gradient rivers of British Columbia. Similarly, Victoriano et al. (2018) determined a MSE of 0.35 m using a total station and a 1D hydraulic model in a single mountain stream in Spain. Other studies have reported deviations similar to those obtained in our study, despite the fact that differential GPS (Ballesteros-Cánovas et al., 2011a) or terrestrial laser scans (Ballesteros-Cánovas et al., 2011b) were used in these cases. On the other hand, a MSE exceeding >1.5 m was obtained for a stream in Bhutan for which high-resolution topographic data was missing (Speer et al., 2019). Interestingly, Garrote et al. (2018) reported MSE exceeding 2 m at a site of the Canary Islands,

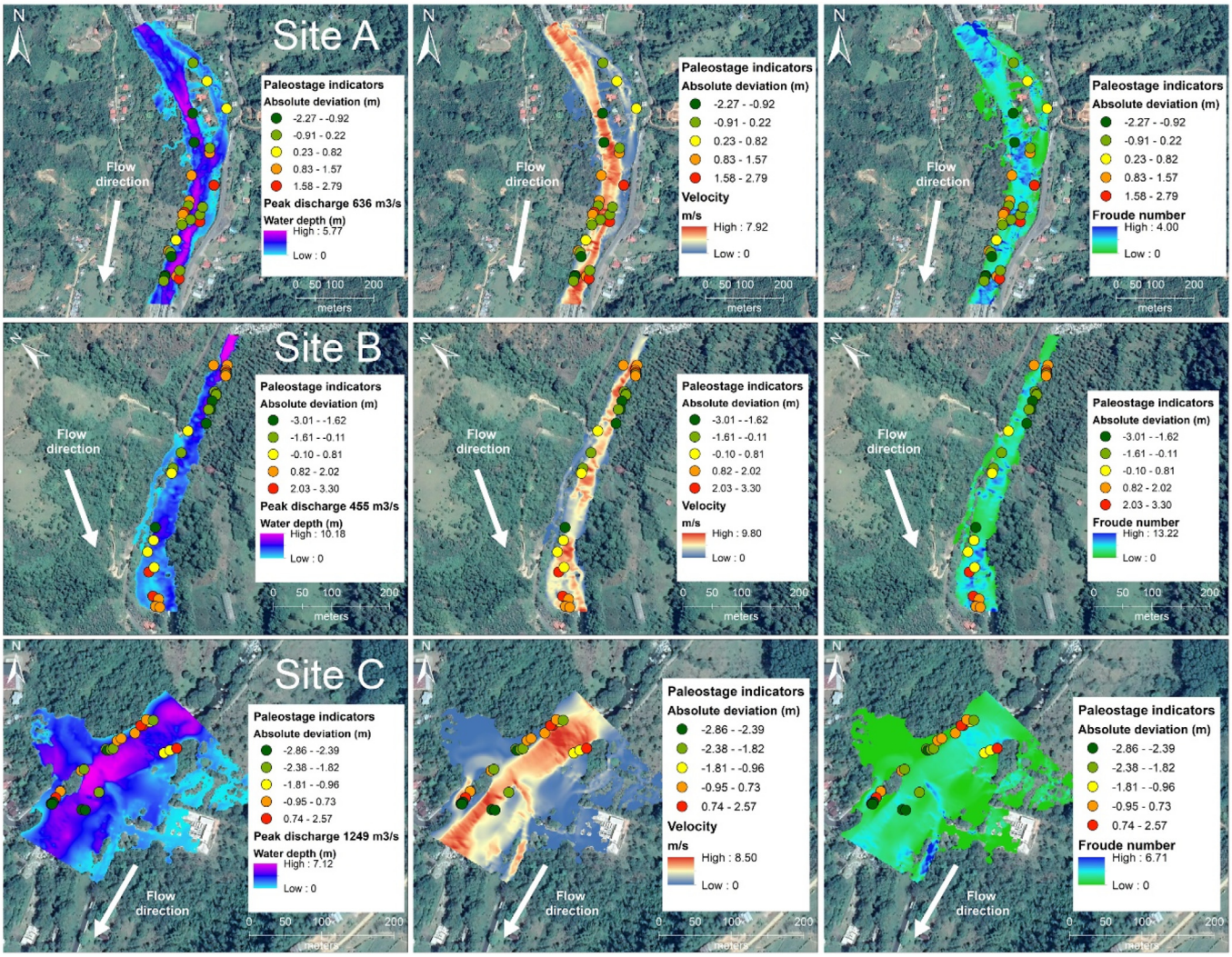

Fig. 4. Absolute deviations (in m) of PSI as observed on tree trunks and modeled with Iber, as well as their relationship with water depth, flow velocity, and Froude number at study reaches A, B, and C of the Río General.

Spain, and with flow magnitudes (1235 m^3/s) comparable to those at our study sites. According to Webb and Jarrett (2002) and Ballesteros-Cánovas et al. (2011b), the creation of impact scars by large wood transported that is partially submerged in the flood flow could explain these deviations in peak discharge. Such dynamics have indeed been observed and documented in tropical channel reaches with high stream power (Cadol et al., 2009), also in relation with tropical cyclones (Wohl et al., 2019). During tropical (flash) floods, wooden logs are easily fragmented into pieces and may crash against standing trees (Cadol and Wohl, 2010).

Table 2
Parameters used to model peak discharge of the 2017 flood. The residual standard error is 0.15 on 77° df, the multiple R-squared is 0.62, and the AIC is 34.86. *Pr*(>|z|) is the probability of finding the observed *Z*-ratio in the normal distribution of Z with a critical point of |z|. ***$P = .001$ and *$P = .05$.

Model terms	Estimate	Std. Error	t value	*Pr*(>|t|)	
(Intercept)	1.30	0.03	35.38	<0.001	***
Landform PB	0.06	0.05	1.34	0.18	
Landform SC	0.09	0.04	2.24	0.02	*
Site B	0.45	0.05	10.63	<0.001	***
Site C	0.35	0.04	8.21	<0.001	***

5.2. Reliable geomorphic locations of trees

One of the main weaknesses of dendrogeomorphic approaches is the substantial time required for an exhaustive sampling of a site and geomorphic process (Mainieri et al., 2019). Therefore, it seems essential to identify the landforms for which scar heights in trees deviate least from modeled flow heights. As previously speculated by Ballesteros-Cánovas et al. (2011a), we confirm that the geomorphic position of trees is the main factor explaining deviations between models and field observations. It is also known that mean heights of scars in trees located in overbank positions are smaller than scar heights in trees standing within the main channel (Gottesfeld, 1996; Yanosky and Jarrett, 2002). More recently, Victoriano et al. (2018) found that landforms characterized by intermediate energy, such as alluvial terraces, are more reliable for a sampling of scars to estimate peak discharge, as riparian vegetation growing in such a context would have a better biogeomorphic resilience against streambank erosion (Abernethy and Rutherfurd, 2001; Stallins and Corenblit, 2018). Field observations confirm that smaller floods modify or erode point bars and straight channels morphologies and their vegetation more easily (Simon and Collison, 2002; Polvi et al., 2014). Our results indicate that trees standing on point bars and in straight channels are affected by higher flow velocities and Froude numbers in the model. A systematic sampling of scars

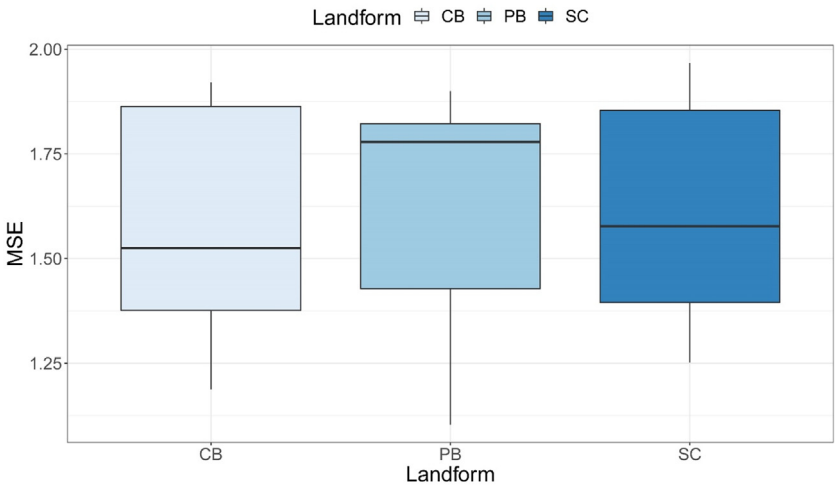

Fig. 5. Boxplots with calculated mean squared error between observed (scars) and modeled peak discharge as a function of geomorphic position of trees. CB–cut bank; PB–point bar; SC–straight channel.

in trees located in more stable landforms, such as cut banks, could reduce significantly the time needed in dendrogeomorphic studies and also improve results.

5.3. Implications for flood risk reduction on tropics

Despite the inherent uncertainties of the method, our assessment provided a peak discharge reconstruction for a flood of the Río General that was triggered by the passage of Tropical Storm Nate in October 2017. The reconstructed peak discharge is in the same order of magnitude as the values obtained by the Electricity Institute of Costa Rica on October 4, 2017 (947 m^3/s), and therefore confirms the suitability of dendrogeomorphic techniques to reconstruct past floods and their magnitude with trees in the tropics. However, the study could have benefitted further from additional post-event surveys that would have helped to reduce the remaining uncertainties that are inherent to flood reconstructions (Quesada-Román et al., 2019a; Wilhelm et al., 2019). The approach used in this study should be replicated in other tropical catchments as an improved understanding of peak discharge in catchments without or with very limited meteorological and/or flow discharge data will always be of paramount importance to increase resilience of local inhabitants and/or to improve infrastructure crossing rivers (i.e., bridges) and flood zoning. Even if tropical areas count for only 19% of the global land surface (Peel et al., 2007), they host between 40 and 50% of the global population (Tatem, 2017). This is even more relevant as emerging countries and smaller economies located in the tropics also often face more difficult economic situations after a disaster and during recovery (Noy, 2009). The practical dendrogeomorphic approach presented here can be a means to improve flood area zonation and thereby assist in the development of more detailed flood hazard and risk maps.

6. Conclusions

In this study we have shown that peak discharge of a recent flood in a poorly gauged tropical mountain catchment can be estimated with dendrogeomorphic techniques if coupled to a 2D hydraulic model and channel topography derived from UAV photogrammetry. As the first study of its kind in the humid tropics, this publication thus expands the geographic scope of tree-ring based hazard analysis. The approach presented here did not only provide results on past peak discharge with limited uncertainly, but also yielded valuable data on flood dynamics that will help to improve our understanding of flood processes in tropical regions. We also find that future research should focus on trees on cut banks or on terraces where deviations between modeled and observed flow heights are minimal. At the same time, we recommend that impacted trees growing on alluvial bars or within straight channel reaches should not be sampled in the future. By limiting differences between reconstructions, direct observations and model outputs, we conclude that dendrogeomorphic approaches are becoming an increasingly important tool for disaster risk reduction and territorial

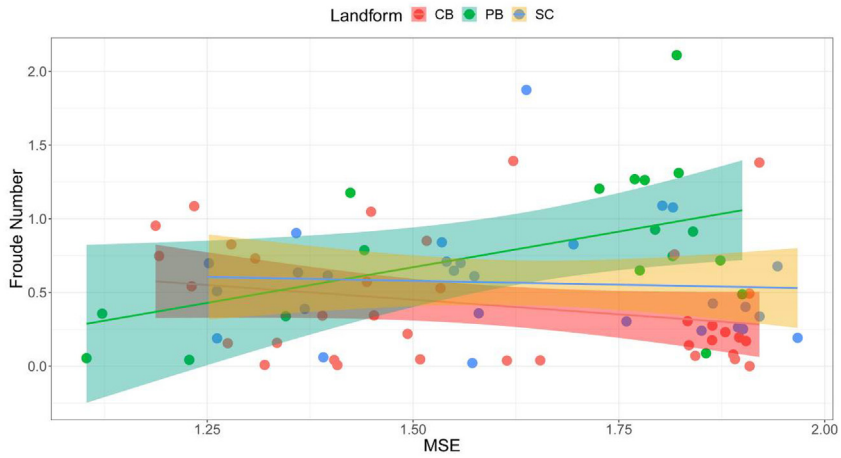

Fig. 6. Relation between Froude number and calculated average mean squared error depending on the geomorphic position (cut bank, straight channel, point bar) of trees with scars.

management decisions in (tropical) regions where data on past events are scarce or rather unreliable.

Declaration of competing interest

All authors have seen and approved the final version of the submitted manuscript. They warrant that the article is the authors' original work, has not received prior publication and is not under consideration for publication elsewhere.

Acknowledgments

We greatly thank to L. Quesada, V. Ruiz-Villanueva, J. Madrigal-Gonzalez, S. Guillet, S. Lecce, and anonymous reviewers for their useful collaboration and suggestions that highly improved the analysis and final manuscript. This work is part of a PhD project of AQR, funded by the Swiss Federal Commission for Scholarships (ESKAS-Nr 2017.1072), Ministry of Science, Technology and Telecommunications of Costa Rica (N°MICITT-PINN-CON-2-1-4-17-1-002), and the University of Costa Rica (OAICE-187-2017).

References

Abernethy, B., Rutherfurd, I.D., 2001. The distribution and strength of riparian tree roots in relation to riverbank reinforcement. Hydrol. Process. 15, 63–79. https://doi.org/10.1002/hyp.152.

Alfaro, E., Quesada-Román, A., Solano, F.J., 2010. Análisis del impacto en Costa Rica de los ciclones tropicales ocurridos en el Mar Caribe desde 1968 al 2007. Rev. Diálogos 11 (2), 25-38. doi:10.15517/dre.v11i2.578.

Anderson, D.R., Burnham, K., 2004. Model Selection and Multi-model Inference. Second edition. Springer-Verlag, New York, p. 488.

Arcement, G.J., Schneider, V.R., 1989. Guide for selecting Manning's roughness coefficients for natural channels and flood plains. United States Geological Survey. Water-Supply Paper 2339.

Baker, V.R., 2008. Paleoflood hydrology: origin, progress, prospects. Geomorphology 101 (1–2), 1–13. https://doi.org/10.1016/j.geomorph.2008.05.016.

Ballesteros-Cánovas, J.A., Bodoque, J.M., Díez-Herrero, A., Sanchez-Silva, M., Stoffel, M., 2011a. Calibration of floodplain roughness and estimation of flood discharge based on tree-ring evidence and hydraulic modelling. J. Hydrol. 403, 103–115. https://doi.org/10.1016/j.jhydrol.2011.03.045.

Ballesteros-Cánovas, J.A., Eguibar, M., Bodoque, J.M., Díez-Herrero, A., Stoffel, M., Gutiérrez-Pérez, I., 2011b. Estimating flash flood discharge in an ungauged mountain catchment with 2D hydraulic models and dendrogeomorphic palaeostage indicators. Hydrol. Process. 25, 970–979. https://doi.org/10.1002/hyp.7888.

Ballesteros-Cánovas, J.A., Czajka, B., Janecka, K., Lempa, M., Kaczka, R.J., Stoffel, M., 2015a. Flash floods in the Tatra Mountain streams: frequency and triggers. Scie. of the Total Environ. 511, 639–648. https://doi.org/10.1016/j.scitotenv.2014.12.081.

Ballesteros-Cánovas, J.A., Stoffel, M., St George, S., Hirschboeck, K., 2015b. A review of flood records from tree rings. Prog. Phys. Geogr. 39 (6), 794–816. https://doi.org/10.1177/0309133315608758.

Ballesteros-Cánovas, J.A., Stoffel, M., Spyt, B., Janecka, K., Kaczka, R.J., Lempa, M., 2016. Paleoflood discharge reconstruction in Tatra Mountain streams. Geomorphology 272, 92–101. https://doi.org/10.1016/j.geomorph.2015.12.004.

Ballesteros-Cánovas, J.A., Trappmann, D., Shekhar, M., Bhattacharyya, A., Stoffel, M., 2017. Regional flood-frequency reconstruction for Kullu district, Western Indian Himalayas. J. of Hydrology 546, 140–149. https://doi.org/10.1016/j.jhydrol.2016.12.059.

Barnes, H.H., 1967. Roughness characteristics of natural channels. United States Geological Survey. Water-Supply Paper 1849.

Beven, J.L., Berg, R., 2018. National Hurricane Center tropical cyclone report: Hurricane Nate. NOAA/NWS Rep.AL162017. p. 45. https://www.nhc.noaa.gov/data/tcr/AL162017_Nate.pdf.

Borga, M., Gaume, E., Creutin, J.D., Marchi, L., 2008. Surveying flash floods: gauging the ungauged extremes. Hydrol. Process. 22 (18), 3883–3885. https://doi.org/10.1002/hyp.7111.

Borga, M., Stoffel, M., Marchi, L., Marra, F., Jakob, M., 2014. Hydrogeomorphic response to extreme rainfall in headwater systems: flash floods and debris flows. J. Hydrol. 518, 194–205.

Brenes, A., Girot, P., 2018. Gestión del riesgo y cambio climático. Informe Estado de la Nación en Desarrollo Humano Sostenible. Pavas, Costa Rica: CONARE, Programa Estado de la Nación, p. 1-52.

Cadol, D., Wohl, E., 2010. Wood retention and transport in tropical, headwater streams, La Selva Biological Station, Costa Rica. Geomorphology 123 (1–2), 61–73. https://doi.org/10.1016/j.geomorph.2010.06.015.

Cadol, D., Wohl, E., Goode, J.R., Jaeger, K.L., 2009. Wood distribution in neotropical forested headwater streams of La Selva, Costa Rica. Earth Surf. Process. Land. 34, 1198–1215. https://doi.org/10.1002/esp.1800.

Camacho, M.E., Quesada-Román, A., Mata, R., Alvarado, A., 2020. Soil-geomorphology relationships of alluvial fans in Costa Rica. Geoderma Regional 21 (1–12), e00258. https://doi.org/10.1016/j.geodrs.2020.e00258.

Campos-Durán, D., Quesada-Román, A., 2017. Impacto de los eventos hidrometeorológicos en Costa Rica, periodo 2000–2015. Rev. Geo UERJ 30, 440–465. doi:10.12957/geouerj.2017.26116

Cea, L., Bladé, E., Sanz-Ramos, M., Bermúdez Pita, M., Mateos-Alonso, Á., 2019. Iber Applications Basic Guide. https://doi.org/10.17979/spudc.9788497497176.

Cervantes-Cordero, R., 1999. Disminución de la escorrentía superficial debido a variaciones en el uso del suelo. Informe de Trabajo de Graduación. Licenciatura en Ingeniería Civil. Escuela de Ingeniería Civil. Universidad de Costa Rica, p. 61.

Chow, V., 1959. Open-channel Hydraulics. McGraw-Hill, New York, p. 680.

CNE - Comisión Nacional de Prevención de Riesgos y Atención de Emergencias, 2018. Plan general de la emergencia ante la situación provocada por la Tormenta Tropical Nate. San José, Costa Rica. p. 23. Accessed in: https://www.cne.go.cr/Documentos/Plan_de_Emergencia_40677.pdf

Díez-Herrero, A., Ballesteros, J.A., Ruiz-Villanueva, V., Bodoque, J.M., 2013. A review of dendrogeomorphological research applied to flood risk analysis in Spain. Geomorphology 196, 211–220. https://doi.org/10.1016/j.geomorph.2012.11.028.

Franco-Ramos, O., Ballesteros-Cánovas, J.A., Figueroa-García, J.E., Vázquez-Selem, L., Stoffel, M., Caballero, L., 2020. Modelling the 2012 Lahar in a Sector of Jamapa Gorge (Pico de Orizaba Volcano, Mexico) using RAMMS and Tree-Ring evidence. Water 12, 333. https://doi.org/10.3390/w12020333.

Garrote, J., Díez-Herrero, A., Génova, M., Bodoque, J., Perucha, M., Mayer, P., 2018. Improving Flood Maps in Ungauged Fluvial Basins with Dendrogeomorphological Data. An example from the Caldera de Taburiente National Park (Canary Islands, Spain). Geosciences 8 (8), 1–18. https://doi.org/10.3390/geosciences8080300.

Goldenberg, S.B., Landsea, C.W., Mestas-Nuñez, A.M., Gray, W.M., 2001. The recent increase in Atlantic hurricane activity: causes and implications. Science 293 (5529), 474–479.

Gottesfeld, A.S., 1996. British Columbia flood scars: maximum flood-stage indicator. Geomorphology 14, 319–325.

Gottesfeld, A.S., Gottesfeld, L.M.J., 1990. Floodplain dynamics of a wandering river: dendrochronology of the Morice River, British Columbia, Canada. Geomorphology 3, 159–179.

Hupp, C.R., 1988. In: 1988 (Ed.), Plant Ecological Aspects of Flood Geomorphology and Paleoflood History. Flood Geomorphology. John Wiley & Sons, New York, pp. 335–356.

ICE – Instituto Costarricense de Electricidad, 2018. Flow Discharge Information of Rivas Station. Centro de Servicios Estudios Básicos de Ingeniería – Hidrología. San José, Costa Rica.

Kappelle, M., 2016. The montane cloud forests of the Cordillera de Talamanca. In: Kappelle, M. (Ed.), Costa Rican Ecosystems. University of Chicago Press, Chicago, p. 774.

Krishnaswamy, J., Kelkar, N., Birkel, C., 2018. Positive and neutral effects of forest cover on dry-season stream flow in Costa Rica identified from Bayesian regression models with informative prior distributions. Hydrol. Process. 32 (24), 3604–3614. https://doi.org/10.1002/hyp.13288.

Lagadec, A., Boucher, É., Germain, D., 2015. Tree ring analysis of hydro-climatic thresholds that trigger ice jams on the Mistassini River. Quebec. Hydrol. Process. 29 (23), 4880–4890. https://doi.org/10.1002/hyp.10537.

Langhammer, J., Vacková, T., 2018. Detection and mapping of the geomorphic effects of flooding using UAV photogrammetry. Pure and Appl. Geoph. 175 (9), 3223–3245. https://doi.org/10.1007/s00024-018-1874-1.

Lawrence, D., Vandecar, K., 2015. Effects of tropical deforestation on climate and agriculture. Nat. Clim. Chang. 5 (1), 27–36. https://doi.org/10.1038/nclimate2430.

Leopold, L.B., Wolman, M.G., Miller, J.P., 1995. Fluvial Processes in Geomorphology. Courier Corporation.

Mainieri, R., Lopez-Saez, J., Corona, C., Stoffel, M., Bourrier, F., Eckert, N., 2019. Assessment of the recurrence intervals of rockfall through dendrogeomorphology and counting scar approach: a comparative study in a mixed forest stand from the Vercors massif (French Alps). Geomorphology 340, 160–171. https://doi.org/10.1016/j.geomorph.2019.05.005.

Maldonado, T., Rutgersson, A., Alfaro, E., Amador, J., Claremar, B., 2016. Interannual variability of the midsummer drought in Central America and the connection with sea surface temperatures. Adv. Geosci. 42, 35–50. https://doi.org/10.5194/adgeo-42-35-2016.

McCord, V.A., 1990 Augmenting flood frequency estimates using flood-scarred trees. PhD Thesis, University of Arizona, Tucson.

NOAA – National Oceanic and Atmospheric Administration, 2019. El Niño and La Niña years and intensities based on Oceanic Niño Index (ONI). https://origin.cpc.ncep.noaa.gov/products/analysis_monitoring/ensostuff/ONI_v5.php (accessed 15 April 2019).

Noy, I., 2009. The macroeconomic consequences of disasters. J. of Develop. Econ. 88 (2), 221–231. https://doi.org/10.1016/j.jdeveco.2008.02.005.

Papin, P.P., Bosart, L.F., Torn, R.D., 2017. A climatology of central American gyres. Mon. Weather Rev. 145 (5), 1983–2000. https://doi.org/10.1175/MWR-D-16-0411.1.

Peel, M.C., Finlayson, B.L., McMahon, T.A., 2007. Updated world map of the Köppen–Geiger climate classification. Hydrol. Earth Syst. Sci. 11, 1633–1644. https://doi.org/10.5194/hess-11-1633-2007.

Perks, M.T., Russell, A.J., Large, A.R., 2016. Advances in flash flood monitoring using unmanned aerial vehicles (UAVs). Hydrol. Earth Syst. Scie. 20 (10), 4005–4015. https://doi.org/10.5194/hess-20-4005-2016.

Polvi, L.E., Wohl, E., Merritt, D.M., 2014. Modeling the functional influence of vegetation type on streambank cohesion. Earth Surf. Proc. Landf. 39 (9), 1245–1258. https://doi.org/10.1002/esp.3577.

Quesada-Román A., 2017. Geomorfología Fluvial e Inundaciones en la Cuenca Alta del Río General, Costa Rica. Anuá. Inst. Geoc. 40 (2), 278–288. doi:10.11137/2017_2_278_288

Quesada-Román, A., Zamorano-Orozco, J.J., 2018. Peligros Geomorfológicos en Costa Rica: Cuenca Alta del Río General. Anuá. Inst. Geoc. 41 (3), 239–251. http://dx.doi.org/10.11137/2018_3_239_251.

Quesada-Román, A., Zamorano-Orozco, J.J., 2019a. Geomorphology of the Upper General River Basin. Costa Rica. J. of Maps 15 (2), 95–101. https://doi.org/10.1080/17445647.2018.1548384.

Quesada-Román, A., Zamorano-Orozco, J.J., 2019b. Zonificación de procesos de ladera e inundaciones a partir de un análisis morfométrico en la cuenca alta del río General, Costa Rica. Inv. Geog., Bol. Inst. Geog. 99, 1–19. https://doi.org/10.14350/rig.56770.

Quesada-Román, A., Fallas-López, B., Hernández-Espinoza, K., Stoffel, M., Ballesteros-Cánovas, J.A., 2019a. Relationships between earthquakes, hurricanes, and landslides in Costa Rica. Landslides 16 (8), 1539–1550. https://doi.org/10.1007/s10346-019-01209-4.

Quesada-Román, A., Stoffel, M., Ballesteros-Cánovas, J.A., Zamorano-Orozco, J.J., 2019b. Glacial geomorphology of the Chirripó National Park. Costa Rica. J. of Maps 15 (2), 538–545. https://doi.org/10.1080/17445647.2019.1625822.

REDD/CCAD-GIZ - SINAC, 2015. Inventario Nacional Forestal de Costa Rica 2014–2015 [National Forestry Inventory of Costa Rica 2014–2015]. Programa Reducción de Emisiones por Deforestación y Degradación Forestal en Centroamérica y la República Dominicana (REDD/CCAD/GIZ) y Sistema Nacional de Áreas de Conservación (SINAC) Costa Rica. San José, Costa Rica. p. 380.

Rodriguez-Morata, C., Ballesteros-Cánovas, J.A., Trappmann, D., Beniston, M., Stoffel, M., 2016. Regional reconstruction of flash flood history in the Guadarrama range (Central System, Spain). Scie. of the Total Environ. 550, 406–417.

Ruiz-Villanueva, V., Díez-Herrero, A., Bodoque, J.M., Ballesteros, J.A., Stoffel, M., 2013. Characterization of flash floods in small ungauged mountain basins of central Spain using an integrated approach. Catena 110, 32–43.

Shroder, J.F., 1978. Dendrogeomorphological analysis of mass movement on Table Cliffs Plateau, Utah. Quat. Res. 9, 168–185.

Sigafoos, R.S., 1964. Botanical Evidence of Floods and Flood-plain Deposition. Professional Paper, 485A. United States Geological Survey, p. 35.

Silva, M.D.S., Funch, L.S., da Silva, L.B., 2019. The growth ring concept: seeking a broader and unambiguous approach covering tropical species. Biol. Rev. 94 (3), 1161–1178. https://doi.org/10.1111/brv.12495.

Simon, A., Collison, A.J.C., 2002. Quantifying the mechanical and hydrologic effects of riparian vegetation on streambank stability. Earth Surf. Proc. Landf. 27, 527–546. https://doi.org/10.1002/esp.325.

Slaymaker, O., Embleton-Hamann, C., 2018. Advances in global mountain geomorphology. Geomorphology 308, 230–264. https://doi.org/10.1016/j.geomorph.2018.02.016.

Smith, D.G., Reynolds, D.M., 1983. Trees scars to determine the frequency and stage of high magnitude river ice drives and jams, Red Deer, Alberta. Canad. Water Res. J. 8 (3), 77–94. https://doi.org/10.4296/cwrj0803077.

Smith, M.J., Paron, P., Griffiths, J.S., 2011. Geomorphological Mapping: Methods and Applications. (Vol. 15). Elsevier, p. 612.

Speer, J.H., Shah, S.K., Truettner, C., Pacheco, A., Bekker, M.F., Dukpa, D., Cook, E.J., Tenzin, K., 2019. Flood history and river flow variability recorded in Tree Rings on the Dhur River, Bhutan. Dendrochronologia 56, 125605. https://doi.org/10.1016/j.dendro.2019.125605.

Stallins, J.A., Corenblit, D., 2018. Interdependence of geomorphic and ecologic resilience properties in a geographic context. Geomorphology 305, 76–93. https://doi.org/10.1016/j.geomorph.2017.09.012.

Stoffel, M., Wilford, D.J., 2012. Hydrogeomorphic processes and vegetation: disturbance, process histories, dependencies and interactions. Earth Surf. Proc. Landf. 37, 9–22. https://doi.org/10.1002/esp.2163.

Syvitski, J.P.M., Cohen, S., Kettner, A.J., Brakenridge, G.R., 2014. How important and different are tropical rivers? - an overview. Geomorphology 227, 5–17. https://doi.org/10.1016/j.geomorph.2014.02.029.

Tatem, A.J., 2017. WorldPop, open data for spatial demography. Scientific Data 4, 1–4. https://doi.org/10.1038/sdata.2017.4.

Turner, D., Lucieer, A., Watson, C., 2012. An automated technique for generating georectified mosaics from ultra-high resolution Unmanned Aerial Vehicle (UAV) Imagery, based on Structure from Motion (SfM) point clouds. Remote Sens. 4 (5), 1292–1410. https://doi.org/10.3390/rs4051392.

Victoriano, A., Díez-Herrero, A., Génova, M., Guinau, M., Furdada, G., Khazaradze, G., Calvet, J., 2018. Four-topic correlation between flood dendrogeomorphological evidence and hydraulic parameters (the Portainé stream, Iberian Peninsula). Catena 162, 216–229. https://doi.org/10.1016/j.catena.2017.11.009.

Webb, R.H., Jarrett, R.D., 2002. One-dimensional estimation techniques for discharges of paleofloods and historical floods. In: House, P.K., Webb, R.H., Baker, V.R., Levish, D.R. (Eds.), Ancient Floods, Modern Hazards: Principles and Applications of Paleoflood Hydrology: Water Science and Application. vol. 5. American Geophysical Union, Washington, D.C, pp. 111–126.

Wheaton, J.M., Fryirs, K.A., Brierley, G., Bangen, S.G., Bouwes, N., O'Brien, G., 2015. Geomorphic mapping and taxonomy of fluvial landforms. Geomorphology 248, 273–295. https://doi.org/10.1016/j.geomorph.2015.07.010.

Wilhelm, B., Ballesteros Cánovas, J.A., Macdonald, N., Toonen, W.H., Baker, V., Barriendos, M., Benito, G., Brauer, A., Corella, J.P., Denniston, R., Glaser, R., Ionita, M., Kahle, M., Liu, T., Luetscher, M., Macklin, M., Mudelsee, M., Munoz, S., Schulte, L., St. George, S., Stoffel, M., Wetter, O., 2019. Interpreting historical, botanical, and geological evidence to aid preparations for future floods. Wiley Interd. Rev.: Water 6 (1), e1318. doi: https://doi.org/10.1002/wat2.1318

Wohl, E., 2006. Human impacts to mountain streams. Geomorphology 79 (3–4), 217–248. https://doi.org/10.1016/j.geomorph.2006.06.020.

Wohl, E., 2008. Hydrology and discharge. In: A. Gupta, (Ed.). Large rivers: Geomorphology and management. John Wiley & Sons, pp. 29–44.

Wohl, E., Barros, A., Brunsell, N., Chappell, N.A., Coe, M., Giambelluca, T., Goldsmith, S., Harmon, R., Hendrickx, J.M.H., Juvik, J., McDonnell, J., Ogden, F., 2012. The hydrology of the humid tropics. Nat. Clim. Chang. 2 (9), 655–662. https://doi.org/10.1038/nclimate1556.

Wohl, E., Hinshaw, S.K., Scamardo, J.E., Gutiérrez-Fonseca, P.E., 2019. Transient organic jams in Puerto Rican mountain streams after hurricanes. River Res. Appl. 35 (3), 280–289. https://doi.org/10.1002/rra.3405.

Yanosky, T.M., Jarrett, R.D., 2002. Dendrochronologic evidence for the frequency and magnitude of paleofloods. In: House PK, Webb RH, Baker VR, et al. (eds) Ancient Floods, Modern Hazards: Principles and applications of paleoflood hydrology, Water Science and Application vol. 5. Washington, DC: American Geophysical Union, pp. 77–89.

Zielonka, T., Holeksa, J., Ciapała, S., 2008. A reconstruction of flood events using scarred trees in the Tatra Mountains, Poland. Dendrochronologia 26 (3), 173–183. https://doi.org/10.1016/j.dendro.2008.06.003.